RAPID COMMUNICATIONS

PHYSICAL REVIEW E VOLUME 53, NUMBER 4 APRIL 1996

Phase-field method for computationally efficient modeling of solidification with arbitrary interface kinetics

Alain Karma and Wouter-Jan Rappel

Department of Physics and Center for Interdisciplinary Research on Complex Systems, Northeastern University, Boston, Massachusetts 02115

(Received 7 November 1995)

We present mathematical results which dramatically enhance the computational efficiency of the phase-field method for modeling the solidification of a pure material. These results make it possible to resolve a smaller capillary length to interface thickness ratio and thus render smaller undercooling and three-dimensional computations accessible. Furthermore, they allow one to choose computational parameters to produce a Gibbs-Thomson condition with an arbitrary kinetic coefficient. The method is tested for dendritic growth in two dimensions with zero kinetic coefficient. Simulations yield dendrites with tip velocities and tip shapes which agree within a few percent with numerical Green's function solutions of the steady-state growth problem.

PACS number(s): 05.70.Ln, 64.70.Dv, 81.30.Fb, 81.10.Aj

There has been a continuing search for new computational methods to solve the formidably difficult class of mathematical problems which govern the formation of interfacial patterns in solidification and other fields [1]. Perhaps the most classic example is the solidification of a pure material from its melt which gives rise to dendrite patterns [2]. This problem is described by the well-known equations

$$\partial_t u = D\nabla^2 u, \tag{1}$$

$$v_n = D(\partial_n u]^- - \partial_n u]^+), \tag{2}$$

$$u_i = -d_0(\theta)\kappa - \beta(\theta)v_n, \tag{3}$$

where $u \equiv (T-T_M)/(L/c_p)$ is the dimensionless temperature field, T_M the melting temperature, L the latent heat of melting, and c_p the specific heat at constant pressure. Equation (3) is a velocity-dependent form of the Gibbs-Thomson condition which incorporates the nonequilibrium kinetics of the interface. Also, v_n, u_i, $\partial_n u]^{\pm}$, κ, $d_0(\theta)$, and $\beta(\theta)$, denote, respectively, the normal interface velocity, the value of u on the interface, the normal derivative of u on the liquid $(+)$ and solid $(-)$ sides of the interface, the interface curvature, the anisotropic capillary length, and the anisotropic interface kinetic coefficient. Far from the interface, $u=-\Delta$, where $\Delta \equiv (T_M - T_\infty)/(L/c_p)$ denotes the dimensionless undercooling and T_∞ the initial temperature of the undercooled liquid.

Several methods have been explored which attempt to solve directly the full time-dependent free-boundary problem (TDFBP) defined by Eqs. (1)–(3). These include the following: a time-dependent boundary integral formulation [3], variational algorithms with [4] and without [5] interface kinetics, and a front tracking method with multiple rotated lattices to minimize grid anisotropy [6]. All these methods have produced dendritic patterns in two dimensions which qualitatively look alike. However, so far, conclusive quantitative tests of the operating state of the dendrite tip have only been reported to our knowledge in Ref. [6], where it was found that reasonably accurate tip velocities could be obtained with four rotated lattices. In general, producing reliable results has remained extremely difficult because of the combined problems of tracking a sharp boundary and resolving small anisotropies. Moreover, with perhaps one exception [4], methods that track a sharp boundary are not easily extendible to three dimensions.

The phase-field approach [7–9] is an alternative method to solve the TDFBP which is rooted in continuum models of phase transitions [10]. Its main ingredient consists in distinguishing between phases with a nonconserved order parameter, or phase field ϕ, which is constant within each phase. This field varies smoothly across a spatially diffuse interfacial region of finite thickness W. Its dynamics is then coupled to that of u in such a way that the equations for the two fields reduce to Eqs. (1)–(3) in the so-called sharp-interface limit of the model, $\kappa W \ll 1$, where the interface is curved on a scale much larger than W. The phase-field treatment of the solid-liquid boundary has the well-recognized advantage that it circumvents the problems of front-tracking inherent to other methods. For this reason, it is relatively straightforward to implement computationally [11–13]. Moreover, it has the important advantage that it can be easily extended to three dimensions. There are, however, two limitations of the phase-field approach which, at present, severely restrict its range of application.

(i) Interface kinetics. The first limitation is that the method can only be used to solve the TDFBP with interface kinetics present in the Gibbs-Thomson condition. Hence, it cannot be used to simulate the important physical limit where the kinetic undercooling βv_n is negligibly small compared to the curvature undercooling $d_0\kappa$. For pure materials, the method is actually most efficient in the opposite limit where βv_n is larger than $d_0\kappa$.

(ii) Capillary length and lattice size. Existing analyses [8,9,11–15] of the sharp-interface limit of the phase-field model assume that u does not vary across the interface thickness. This implies that the magnitude of the variation of u on the scale W, $|\delta u_i| \sim W v_n/D$, should be small compared to βv_n; or that $\beta \gg W/D$. Furthermore, β and d_0 scale, respectively, as $\tau/(\lambda W)$ and W/λ, where τ is the time scale of the ϕ field kinetics and λ is the strength of the coupling constant between u and ϕ. The constraint $\beta \gg W/D$ therefore implies that

$$d_0 \gg W^3/D\tau, \tag{4}$$

which, as we shall see below, can also be obtained by a more rigorous analysis. In practice, since the dendrite tip radius scales as $d_0/g(\Delta)$, where $g(\Delta)$ increases sharply with Δ, this constraint requires phase-field simulations on large lattices. This conclusion is consistent with the results of the recent numerical study of Wang and Sekerka [13]. These authors showed that reliable phase-field simulations of dendritic growth—which are independent of computational parameters and satisfy self-consistently the Gibbs-Thomson condition—are only feasible in a range of large Δ (0.8–1.2) where the tip radius is sufficiently small. Furthermore, even in this range, two-dimensional lattices on the order of 1000×1000 were needed. Extending these computations to three dimensions seems difficult even on the fastest supercomputer.

In this paper, we demonstrate that it is possible to remove the above limitations of the phase-field approach, thereby greatly expanding its range of application. We first show analytically that the approach can be extended to produce a Gibbs-Thomson condition with an arbitrarily small or zero β, and with d_0 subject to a much less stringent constraint than the one imposed by Eq. (4). We then perform quantitative numerical tests of dendrite growth in two dimensions which demonstrate the applicability of the results of our analysis. We present here the essential ingredients of our analysis and the most relevant numerical tests. A more detailed exposition of both will be given elsewhere [16].

Our demonstration is based on an analysis of the sharp-interface limit of the phase-field model of the solidification of a pure material which includes spatial variations of u in the interface region. We consider the anisotropic model defined in two dimensions by the equations

$$\tau(\Theta)\partial_t\phi=[\phi-\lambda u(1-\phi^2)](1-\phi^2) \tag{5}$$

$$+\vec{\nabla}\cdot[W(\Theta)^2\vec{\nabla}\phi]-\partial_x[W(\Theta)W'(\Theta)\partial_y\phi]$$
$$+\partial_y[W(\Theta)W'(\Theta)\partial_x\phi],$$

$$\partial_t u=D\nabla^2 u+\partial_t p(\phi)/2, \tag{6}$$

where $\Theta\equiv\arctan(\partial_y\phi/\partial_x\phi)$ is the angle that the directions normal to the contours of constant ϕ make with the x axis. The solid and liquid phases correspond, respectively, to $\phi=+1$ and $\phi=-1$ which are spatially uniform fixed points of Eq. (5). $p(\phi)=\phi$ is the simplest function which incorporates latent heat production at the interface, while, for $p(\phi)=15(\phi-2\phi^3/3+\phi^5/5)/8$, Eqs. (5) and (6) reduce to the entropy formulation [15] used in the computations of Refs. [12,13]. We have found that, for the purpose of using Eqs. (5) and (6) to *solve* the TDFBP, both choices are equally good with the first one being more efficient. For clarity, we first carry out the analysis of the sharp-interface limit in one dimension and then generalize our result to a curved interface. A more formal, but completely equivalent, derivation of this limit which involves the interface Péclet number WV/D as one of the key small parameters in a matched asymptotic expansion will be given in Ref [16].

In the inner region, where $x\sim W$, we look for traveling solutions of Eqs. (5) and (6) in a frame moving with the interface at its instantaneous velocity V (in the $+x$ direction):

$$\tau V\partial_x\phi+W^2\partial_x^2\phi+[\phi-\lambda u(1-\phi^2)](1-\phi^2)=0, \tag{7}$$

$$V\partial_x u+D\partial_x^2 u-V\partial_x p(\phi)/2=0, \tag{8}$$

where we have let $\tau(0)=\tau$ and $W(0)=W$ for brevity of notation. For $V=0$, we obtain trivially the stationary solutions $\phi_0(x)=-\tanh(x/\sqrt{2}W)$ and $u_0(x)=0$. We now look perturbatively for solutions of the form $\phi(x)=\phi_0(x)+\delta\phi(x)$ and $u(x)=\delta u(x)$ for small V. The three terms on the left-hand side of Eq. (8) are of order $V\delta u/W$, $D\delta u/W^2$, and V/W, respectively. In the limit where $\delta u\ll 1$ and $WV/D\ll 1$, the first term is negligibly small compared to the second and third term. We therefore easily find that the solution of Eq. (8) is given by

$$\delta u(x)=\bar{u}+D^{-1}Ax+\frac{VD^{-1}}{2}\int_0^x dx' p(\phi_0(x')), \tag{9}$$

where $\bar{u}$ and A are two constants of integration determined by matching $\delta u(x)$ to the outer solutions of u, denoted by u^+ (u^-) in the solid (liquid) phase. In the outer region $|x|\gg W$, $u^\pm$ simply obey the one-dimensional diffusion equation $\partial_t u^\pm=D\partial_x^2 u^\pm$ since $\partial_t\phi=0$. Thus, in the matching region $W\ll|x|\ll D/V$, $u^\pm$ take the form $u^\pm(x)=u_i+\partial_x u]^\pm x$ where u_i and $\partial_x u]^\pm$ are, respectively, the interfacial undercooling and the normal gradients of u on each side of the interface, in the sharp-interface limit. Letting $\delta u(x)=u^\pm(x)$ for $W\ll\pm x\ll D/V$, yields the conditions: $A=V/2+D\partial_x u]^+$, $A=-V/2+D\partial_x u]^-$, and $u_i=\bar{u}+VD^{-1}F/2$ with $F=\int_0^\infty[p(\phi_0(x))+1]dx$. Eliminating A between the first two conditions yields $V=D(\partial_x u]^- -\partial_x u]^+)$, which is the usual mass conservation condition Eq. (2). We now need an extra condition on $\bar{u}$ to determine u_i. The latter is obtained by substituting $\phi=\phi_0+\delta\phi$ and $u=\delta u$ in Eq. (7) which becomes

$$[W^2\partial_x^2+1-3\phi_0^2]\delta\phi=[\lambda\delta u(1-\phi_0^2)^2-\tau V\partial_x\phi_0]. \tag{10}$$

Since $\partial_x\phi_0$ is a homogeneous solution of Eq. 10, the right-hand side of this equation must be orthogonal to this function for a solution $\delta\phi$ to exist. This solvability condition yields the expression $u_i=-\beta V$ with the kinetic coefficient,

$$\beta=\frac{I}{\lambda J}\frac{\tau}{W}\left[1-\lambda\frac{W^2}{2D\tau}\frac{K+JF}{I}\right], \tag{11}$$

where I, J, and K are constants resulting from the solvability integrals. The numerical values of the various constants are given by $I=2\sqrt{2}/3$ and $J=16/15$, independent of the choice of $p(\phi)$; $K=0.13604$ and $F=\sqrt{2}\ln 2$ for $p(\phi)=\phi$; and $K=0.22359$ and $F=0.49412$ for $p(\phi)=15(\phi-2\phi^3/3+\phi^5/5)/8$. Note that the term Ax in Eq. (9) is odd in x and its integral product in the solvability condition generated by Eq. (10) vanishes identically. This miraculous property explains why u_i does not contain gradient corrections $\sim\partial_x u]^\pm$ as one might have naively expected. The generali-

TABLE I. Comparison of steady-state tip velocities calculated by phase-field simulations ($\tilde{V}_{tip}=d_0V_{tip}/D$) and calculated by the Green's function method ($\tilde{V}_{tip}^{GF}=d_0V_{tip}^{GF}/D$). T_{CPU} denotes the CPU time in hours for simulations on a DEC Alpha 3000-700 workstation. T_{CPU} on one processor of the CRAY C90 is roughly 5 times smaller.

Δ	d_0/W	$\tilde{V}_{tip}$	$\tilde{V}_{tip}^{GF}$	% Error	N_x	N_y	T_{CPU}
0.55	0.277	0.0168	0.0170	1	1300	200	12
0.55	0.185	0.0175	0.0170	3	900	200	3
0.55	0.139	0.0174	0.0170	2	600	150	0.5
0.45	0.185	0.00557	0.00545	2	1500	300	40
0.45	0.139	0.00540	0.00545	1	1300	250	15

zation of the above result to a curved interface in two dimensions is straightforward. It is easy to show that curvature introduces corrections of order $\kappa D\,\delta u/W$ which do not affect the solution of the u field in the inner region as long as $\kappa W\ll 1$. Furthermore, curvature introduces corrections of order κ which, via the above solvability condition, yield the standard anisotropic curvature undercooling term in the Gibbs-Thomson condition derived in Ref. [14]. After a straightforward calculation [16], we find that, Eqs. (5) and (6) reduce in the sharp-interface limit to Eqs. (1)–(3) with

$$d_0(\theta)=\frac{I}{\lambda J}[W(\theta)+W''(\theta)], \tag{12}$$

$$\beta(\theta)=\frac{I}{\lambda J}\frac{\tau(\theta)}{W(\theta)}\left[1-\lambda\frac{W(\theta)^2}{2D\tau(\theta)}\frac{K+JF}{I}\right]. \tag{13}$$

The term in square brackets on the right-hand-side of Eq. (13) represents the correction to the interface kinetic coefficient arising from the variation of u in the interface thickness. It is the main result of this paper which makes it possible to extend the phase-field approach. In the limit where $\lambda W^2/D\tau\ll 1$, this term reduces to unity, as in previous analyses of the sharp-interface limit which assume that u is constant [8,9,11–15]. Since Eq. (12) implies that $d_0\sim W/\lambda$, this limit is equivalent to $d_0\gg W^3/D\tau$, which is exactly the condition [Eq. (4)] of validity of the sharp-interface limit with constant u. In contrast, the validity of Eq. (13) is not subject to this constraint on d_0. We note that there are still four constraints: $|\kappa|W\ll 1$, $W|v_n|/D\ll 1$, $\lambda|u|(1-\phi^2)^2\ll 1$, and $\tau|v_n|/W\ll 1$, which originate from the assumptions made in deriving the sharp-interface limit, and which depend generally on growth conditions. However, these can be shown to be generally much less restrictive on d_0 than Eq. (4), especially for small Δ [16]. Furthermore, since $(K+JF)/I$ is a positive constant, the kinetic coefficient $\beta(\theta)$ can be adjusted at will by varying the ratio $\lambda W(\theta)^2/D\tau(\theta)$. In particular, with the definitions $W(\theta)=Wf_W(\theta)$ and $\tau(\theta)=\tau f_\tau(\theta)$, it can be made to *vanish* by choosing $f_\tau(\theta)=f_W(\theta)^2$ and

$$\lambda=\frac{I}{K+JF}\frac{2D\tau}{W^2}. \tag{14}$$

We report the results of numerical tests of our approach for the interesting case of zero kinetic coefficient. Results shown here are for $p(\phi)=\phi$. Equations (5) and (6) were discretized using standard second order finite difference formulae, except $\nabla^2\phi$ which was discretized using a nine-point formula with nearest and next nearest neighbors which reduces the grid anisotropy. The ϕ and u fields were time-stepped using, respectively, a first order Euler scheme and a second order implicit Crank-Nicholson scheme. Simulations of dendritic growth were performed on two-dimensional lattices of varying dimensions $N_xh\times N_yh$. We used a simple fourfold crystalline anisotropy function, $f_W(\theta)=1+\epsilon\cos 4\theta$ and chose $f_\tau(\theta)$ and λ such that $\beta(\theta)=0$ as described above. All simulations were performed for fixed values of $\epsilon=0.05$, $\tau=1$, $W=1$, $h=0.4$, and $\Delta t=0.016$. The value of h was selected by performing simulations with decreasing h in steps of 0.1 until V_{tip} did not change in value by more than one or two percent. Runs were performed for different values of d_0 by varying D, and hence λ via Eq. (14), and for two different values of Δ. Simulations were seeded with a small quarter disk of solid at one corner of the lattice and a spatially uniform undercooling $u=-\Delta$. N_x was chosen sufficiently large to outlast dynamical transients and for the tip velocity to reach a steady-state value V_{tip}.

In order to benchmark our simulation results, we solved independently the steady-state growth problem defined by Eqs. (1)–(3) with $\partial_t u=-V_{tip}\partial_x u$. This can be done accu-

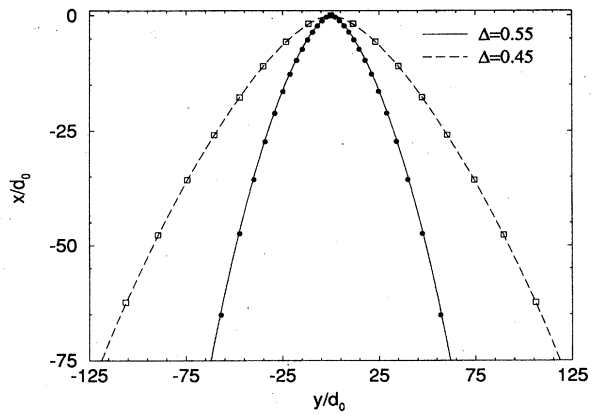

FIG. 1. Comparison of steady-state tip shapes calculated by phase-field simulations (lines) and the Green's function method (symbols). The two interfaces correspond to the following: $\Delta=0.55$, $d_0/W=0.277$ (solid line and circles), and $\Delta=0.45$, $d_0/W=0.185$ (dashed line and squares). For clarity, only one out of every four symbols along the interface is shown for the Green's function results. We have also checked that the addition of noise produces sidebranching (which is absent here) in agreement with theoretical expectations [2].

rately using the standard boundary integral Green's function approach used in Refs. [17]. The input parameters of these calculations were chosen to correspond exactly to those of the phase-field computations; namely $\beta(\theta)=0$, and $d_0(\theta)=d_0(1-15\epsilon\cos 4\theta)$ with $d_0 \equiv WI\lambda^{-1}J^{-1}$ [see Eq. (12)]. A comparison of the dimensionless steady-state tip velocities obtained by phase-field simulations and Green's function calculations is shown in Table I. A comparison of interface shapes is shown in Fig. 1. It can be seen that the quantitative agreement is remarkably good over the whole range of d_0 and Δ investigated here. This is a clear quantitative verification of microscopic solvability theory with a full dynamical phase-field simulation. Table I shows that accurate simulations are still possible at a very small d_0/W ratio with an enormous gain in computational efficiency. This gain can be estimated by noting that the CPU time scales as $\sim N_x N_y \rho_{\rm tip}^2/D\Delta t$ (for the intermediate range of Δ studied here), where $\rho_{\rm tip}^2/D$ is the transient time necessary to reach a steady-state dendrite. Since N_x and N_y can be increased proportionally to $\rho_{\rm tip}/\Delta x$ and $\rho_{\rm tip}\sim d_0$, this time scales roughly as $(d_0/W)^4$. Quantitative three-dimensional simulations of dendritic growth which take full advantage of the cubic anisotropy to reduce computations require about 100 times more CPU time. We have already checked that such simulations are indeed feasible for smaller d_0/W ratio and further computations are currently underway.

In summary, we have presented an analysis of the sharp-interface limit of the phase-field model of a pure material which includes temperature variations across the interface thickness. This analysis extends the phase-field method in two important ways. Firstly, it allows for more efficient computations with a smaller capillary length to interface thickness ratio. This, in turn, renders quantitative three-dimensional simulations directly accessible, as well as the exploration of a much wider range of parameters (undercooling, anisotropy etc.) with the same computational resources. Secondly, it makes it possible to study the physically relevant limit of small or zero kinetic coefficient, which had previously been thought to be unreachable by this method. We have demonstrated the applicability of our results in two dimensions by performing direct quantitative tests of dendrite velocity and shape selection. Simulations yield tip velocities which are very accurate. This insight into the phase-field method should find a wide range of applications in solidification as well as other related interfacial pattern formation phenomena which are governed by similar free-boundary problems.

We thank Herbert Levine for providing the Green's function steady-state code used to benchmark our computations. This research was supported by US DOE Grant No DE-FG02-92ER45471 and benefited from supercomputer time allocation at NERSC.

[1] *Computational Crystal Grower Workshop*, AMS Selected Lectures in Mathematics, edited by Jean Taylor (American Mathematical Society, Providence, RI, 1992).

[2] J. S. Langer, in *Chance and Matter*, Lectures on the Theory of Pattern Formation, Les Houches, Session XLVI, edited by J. Souletie, J. Vannimenus, and R. Stora (North-Holland, Amsterdam, 1987), pp. 629–711; D. Kessler, J. Koplik, and H. Levine, Adv. Phys. **37**, 255 (1988).

[3] J. A. Sethian and J. Strain, J. Comput. Phys. **98**, 2313 (1992).

[4] A. R. Roosen and J. E. Taylor, J. Comput. Phys. **114**, 113 (1994).

[5] R. Almgren, J. Comput. Phys. **106**, 337 (1993).

[6] T. Ihle and H. Muller-Drumbhaar, Phys. Rev. E **49**, 2972 (1994).

[7] G. J. Fix, in *Free Boundary Problems: Theory and Applications, Vol. II*, edited by A. Fasano and M. Primicerio (Piman, Boston, 1983), p. 580.

[8] J. S. Langer, in *Directions in Condensed Matter* (World Scientific, Singapore, 1986), p. 164.

[9] J. B. Collins and H. Levine, Phys. Rev. B **31**, 6119 (1985).

[10] B. I. Halperin, P. C. Hohenberg, and S-K. Ma, Phys. Rev. B **10**, 139 (1974).

[11] R. Kobayashi, Physica D **63**, 410 (1993).

[12] A. A. Wheeler, B. T. Murray, and R. Schaefer, Physica D **66**, 243 (1993).

[13] S-L. Wang and R. F. Sekerka, Phys. Rev. E **53**, 3760 (1996).

[14] G. B. McFadden, A. A. Wheeler, R. J. Braun, S. R. Coriell, and R. F. Sekerka, Phys. Rev. E **48**, 2016 (1993).

[15] S-L. Wang, R. F. Sekerka, A. A. Wheeler, B. T. Murray, S. R. Coriell, R. J. Braun, and G. B. McFadden, Physica D **69**, 189 (1993).

[16] A. Karma and W-J. Rappel (unpublished).

[17] D. A. Kessler and H. Levine, Phys. Rev. B **33**, 7687 (1986); D. I. Meiron, Phys. Rev. A **33**, 2704 (1986).